Naftali (Tuli) Herscovici
AnTeg
52 Agnes Drive
Framingham, MA 01901 USA
Tel: +1 (508) 788-5152
Fax: +1 (508) 788-6226
E-mail: tuli@ieee.org

Christos Christodoulou
Department of Electrical and
Computer Engineering
University of New Mexico
Albuquerque, NM 87131-1356 USA
Tel: +1 (505) 277-6580
Fax: +1 (505) 277-1439
E-mail: christos@eece.unm.edu

Azimuth, Elevation, and Time-Delay Distributions in Wireless Communication Channels

N. Blaunstein[1], M. Toeltsch[2], C. G. Christodoulou[3], J. Laurila[4], E. Tsalolihin[1], E. Bonek[2], P. Vainikainen[4], N. Tsouri[1], K. Kalliola[4], and H. Laitinen[4]

[1]Department of Communication Systems Engineering
Ben Gurion University of the Negev, Beer Sheva, Israel

[2]Institut für Nachrichtentechnik und Hochfrequenztechnik, Technische Universität Wien
Vienna, Austria

[3]Electrical and Computer Engineering Department, University of New Mexico
Albuquerque, NM, USA

[4]Helsinki University of Technology, Espoo; Nokia NRC
Finland

Abstract

We investigate the wave-propagation characteristics in urban environments as functions of the angle-of-arrival distribution, both in the azimuth and elevation planes. We also take into consideration the time delays for various base-station antenna elevations. We combine a statistical multi-parametric model, describing randomly distributed buildings, and a waveguide model, describing a grid of crossing streets with buildings lining the sides to create a new stochastic model. The joint probability of signal distributions in the azimuth-elevation, azimuth-time delay, and elevation-time delay planes are obtained and compared with high-resolution three-dimensional experiments carried out in urban areas in Helsinki, Finland. A good agreement between experimental and theoretical results is obtained.

Keywords: Land mobile radio cellular systems; multibeam antennas; smart antennas; MIMO; Land mobile radio diversity systems; Land mobile radio propagation factors; delay effects; delay estimation; communication channels

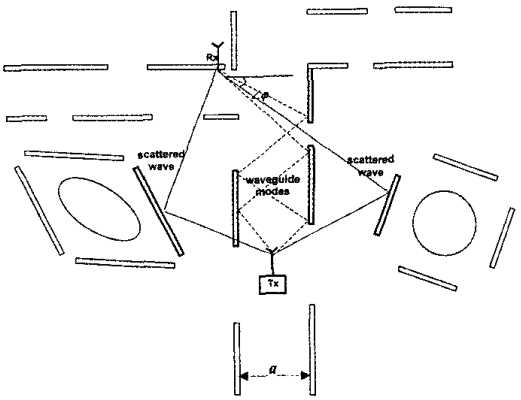

Figure 1. A two-dimensional model of the street waveguide accompanied by scatterers randomly distributed around the transmitter and receiver.

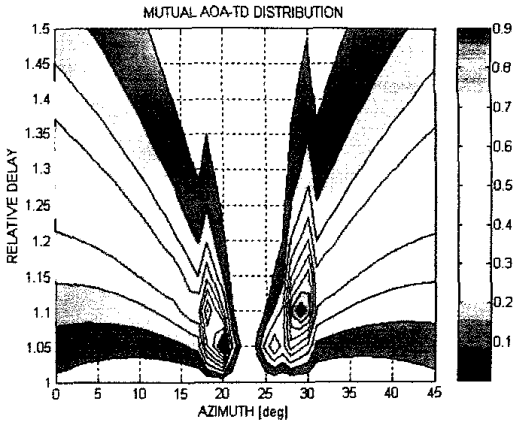

Figure 4. The simulation results of the joint PDF: the antenna is below the rooftop level.

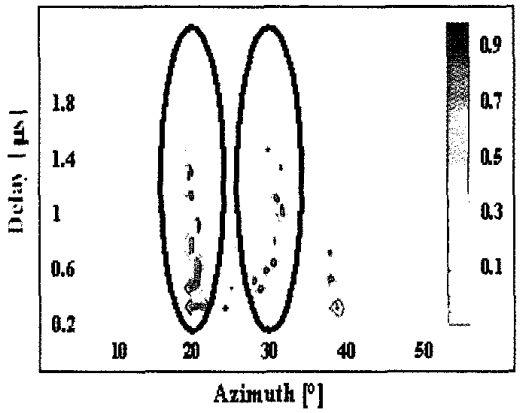

Figure 3. The measurement results in the AOA-TD plane: the antenna is below the rooftop level.

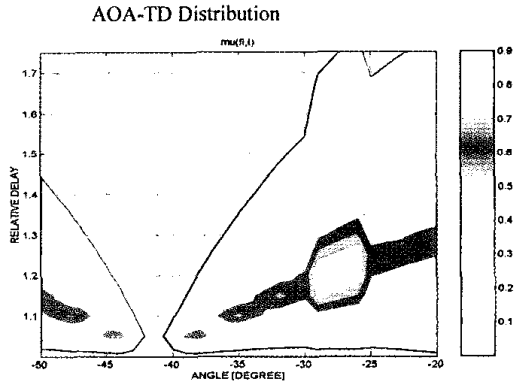

Figure 7. The simulation results: the antenna is on the rooftop level.

1. Introduction

The demand for increased capacity in wireless networks has motivated channel designers toward the development of adaptive (*smart*) techniques to achieve better system performance and higher spectrum efficiency. Different channel models, describing different propagation mechanisms, can be found in the open literature [1-10]. These mechanisms, which govern radio propagation, are complex and diverse.

The main goal of numerous theoretical and experimental investigations is to find more applicable and effective channel models that can describe most physical phenomena related to radio propagation in urban communication settings, in terms of angle-of-arrival, azimuth (AOA) and elevation (EOA), and time delay (TD) distributions of the total field at the receiver. The potential "clients" of a good channel propagation model can be the designers of adaptive antennas, and those who make use of spatial and temporal antenna diversity [11-14]. The channel model should not only be capable of describing the joint AOA, EOA, and TD distributions of the total signal, but should also account for different urban scenarios covering various parameters, such as building heights, building density, and real street orientation.

Investigating the problems of indoor propagation, Spencer [3] proposed a simple concept, based on a clustering model, for both separate and mutual AOA and TD characteristics developed by Saleh and Valenzuela [7]. Spencer's concept was a simple statistical two-dimensional approach that belongs to an empirically-based channel model. This model is used by indoor wireless system designers, but it is insufficient for outdoor urban propagation environments, where the height relationship between the transmitter and the receiver positions is important, and various built-up terrain influences become significant.

The first satisfactory radio propagation model for urban environments was that proposed by Liang, Cheon, and Bertoni, based on the well-known deterministic Vertical Plane Launching (VPL) simulation (ray-launching method) [5, 6]. The VPL technique is capable of determining the three-dimensional (3-D) ray paths that travel between a transmitter and a receiver as the rays undergo multiple reflections and diffractions. The VPL ray-tracing algorithm was originally developed for path-loss prediction purposes, and was later extended to describe TD and AOA signal distributions by means of the Monte Carlo method. Such a numerical tool was used in [5, 6] to define the delay and azimuth signal power distribution by using the second-order moment of the average impulse response. Andersen [4] has proposed a simple statistical two-dimensional model for outdoor propagation channels, taking into account the multiple scattering from the obstructions surrounding a base-station (BS) antenna. This model covered the existing indoor statistical models [4, 7] for all cases of low to high elevation of terminal antennas.

A statistical approach was also proposed in [1, 2] as a measurement-based multipath model, which included the angle-of-arrival and delay-spread distributions. However, in all of the above-mentioned models, the effects of the terrain features and the antenna position with respect to the surrounding obstructions was not taken into consideration. Obviously, an accurate prediction analysis, based on the existing methods, requires a lot of measurements to be produced, with different types of calibration techniques and for different types of propagation environments.

This paper introduces a different approach for handling urban-propagation mechanisms, based on three-dimensional high-resolution radio-channel measurements carried out in different European cities, particularly in Helsinki [11-13]. This approach has analyzed the propagation mechanism using a comprehensive classification of different types of wave propagation in urban environments. Here, three propagation classes are considered: a) the street-guided propagation case (class 1), direct propagation over the rooftop level (class 2), and, finally, scattering and reflection from high-rise objects (class 3).

In [9], a multi-parametric stochastic approach was proposed to handle the AOA and TD signal distribution in urban environments for various elevations of base-station antennas. Here, we show how this stochastic approach can be generalized and used to tackle the joint AOA, EOA, and TD distributions through experiments carried out in Helsinki [11-13]. Several simulation results are presented and compared with experimental data to prove the validity of the new model.

2. Stochastic Approach

In this section, we briefly re-introduce the multi-parametric stochastic model for propagation in a built-up terrain, obtained in [9]. Next, we present the guiding effect caused by a (multi-slit) street waveguide model, and the effects of directional radiation patterns for base-station antennas on the overall signal distribution.

2.1 Azimuth-of-Arrival and Time Delay Distributions for an Array of Buildings Randomly Distributed over a Rough Built-Up Terrain

To fully describe the built-up terrain and the antenna elevations, the following parameters have been introduced, according to the proposed stochastic model [9].

The average horizontal distance of line of sight (LOS), $\gamma_0^{-1} = \langle \rho \rangle$, is defined as

$$\gamma_0^{-1} = \langle \rho \rangle = \frac{\pi}{2\langle L \rangle \nu}. \quad (1)$$

The minimum and maximum building heights in the area of investigation are h_1 and h_2, and the corresponding terminal antenna heights for the base station (BS) and mobile station (MS), are z_2 and z_1, respectively, with $z_2 > z_1$. In Equation (1) $\langle L \rangle$ denotes the average length of the buildings, and ν is the building density per square kilometer.

Using the results obtained in [9, 14] and the parameters introduced above, the density distribution of scattering points (from buildings) can be presented as

$$\mu(\tau,\varphi)=0.5\nu\sin^2\left(\frac{\alpha}{2}\right)\left[\gamma_0\bar{h}\frac{d^2\left(\tau^3-\tau\right)}{2(\tau-\cos\varphi)}\right.$$
$$\left.\frac{\exp\left\{-\gamma_0\left[\frac{\tau^2 d\left(z_2+\bar{h}\right)-2\tau d z_2\cos\varphi+d\left(z_2-\bar{h}\right)}{2z_2(\tau-\cos\varphi)}\right]\right\}}{z_2}\right]$$
$$+0.5\nu\sin^2\left(\frac{\alpha}{2}\right)\left\{\left(z_2-\bar{h}\right)\frac{d\left(\tau^2-2\tau\cos\varphi+1\right)}{2(\tau-\cos\varphi)}\right.$$
$$\left.\frac{\exp\left[-\gamma_0\frac{d\left(\tau^2-2\tau\cos\varphi+1\right)}{2(\tau-\cos\varphi)}\right]}{\bar{h}}\right\} \quad (2)$$

where $\bar{h}$ is an average building height, φ is the azimuth angle, and α is the angle between the ray from the base station to the scatterer (in our case, a building) and the ray from the scatterer to the mobile station. d is the range between the transmitter and the receiver (called the "pseudo-LOS" distance). The relative time, τ, of signal arrival, $\tau=\frac{(r+\tilde{r})}{d}$, is given by

$$r(\tau,\varphi)=\frac{d\left(\tau^2-1\right)}{2(\tau-\cos\varphi)}$$

and

$$\tilde{r}(\tau,\varphi)=\frac{d\left(\tau^2-2\tau\cos\varphi+1\right)}{2(\tau-\cos\varphi)}.$$

2.2 Field-Intensity Attenuation in a Street Waveguide Model

This concept is based on the idea that EM waves propagate along the streets in a city area as if the street were structured in the form of a broken (multi-slit) waveguide [8]. This model considers multiple reflections from building walls, multiple diffractions from buildings' corners, and reflections from the road surface. The street is considered to be a multi-slit (broken) waveguide, with a Poisson distribution for the buildings in the street and the intervals between them (slits). Using [14], we present this PDF, $\mu(r)_{wg}$, as

$$\mu(r)_{wg}=\exp\left[-2\frac{|\ln\chi|}{a'}r\right], \quad (3)$$

where

$$a'=\sqrt{\frac{4a^4}{\lambda^2 n^2}+a^2}; \quad (4)$$

r is the base-station to mobile-station distance; χ is a brokenness parameter, defined by

$$\chi=\frac{\langle L\rangle}{\langle L\rangle+\langle l\rangle}; \quad (5)$$

a is the width of a street; and n is a number of reflections (wave modes).

2.3 AOA and TD Distributions Affected by a Multi-Slit Street Waveguide

In this section, we account for the guiding effect empirically found in [11-13] during a number of experiments in the urban environment. Two distributions are of interest here. The first distribution is $\mu(r,\varphi)$, according to Equation (2), which describes the general spatial distribution of rays scattered by buildings that surround both terminal antennas. The second distribution is $\mu(r)_{wg}$, according to Equation (3), which describes the wave modes caused by the multi-slit street waveguide at distance r from the transmitter. From the geometry shown in Figure 1, the dependence of a' on angle φ is given by $a'(\varphi)=\frac{2a^2(\varphi)}{\lambda}$, with $\frac{4a^4}{\lambda^2}\gg a^2$ and $n=1$; $a(\varphi)$ is determined for each discrete angle φ. The expression for the joint PDF is

$$\mu(r,\varphi)_{wg}=\exp\left[-2\frac{|\ln\chi|}{a'(\varphi)}r\right]. \quad (6)$$

Let us examine the correlation between $\mu(r,\varphi)$ and $\mu(r,\varphi)_{wg}$. These two functions are largely independent, because they are describing two different physical phenomena. If so, the completed form of the joint AOA and TD distribution of the scattered and guided waves can be written as a simple multiplication of these two functions. For this, as in Section 2.1, we can introduce the relative time, τ, instead of distance r:

$$\mu_{fin}=\mu(\tau,\varphi)\mu(\tau,\varphi)_{wg}. \quad (7)$$

Substituting the appropriate functions for $\mu(\tau,\varphi)$ and $\mu(\tau,\varphi)_{wg}$, we can rewrite Equation (7) as

$$\mu_{fin}(\tau,\varphi)=$$
$$0.5\gamma_0\nu\sin^2\left(\frac{\alpha}{2}\right)\tau d\exp\left(-\gamma_0\tau d\right)\exp\left[-2\frac{|\ln\chi|}{a'(\varphi)}\frac{d\left(\tau^2-1\right)}{2(\tau-\cos\varphi)}\right]. \quad (8)$$

Equation (8) is valid for the typical urban situation when both the receiving (RX) and transmitting (TX) antennas are placed below the rooftop level of the buildings or at the rooftop level. The AOA distribution, $\mu_{fin}(\varphi)$, can be obtained by integrating Equation (8) using a new variable, $\tau\in(1,\infty)$, which describes the relative time-delay parameter normalized to the pseudo-LOS distance.

The corresponding TD distribution, $\mu_{fin}(\tau)$, can be derived by integrating Equation (8) using the appropriate angle variable $\varphi \in (-\pi, \pi)$. The calculation of the accepted integrals can be performed using numerical methods.

2.4 Effects of Antenna Directivity in the Elevation-Angle Domain

To find the antenna directivity effects in the elevation-angle domain, we use the von Mises PDF [14], which fully describes the behavior of a directional antenna. Let us denote the elevation angle by the variable θ, and the antenna tilt angle by β ($\beta > 0$ corresponds to a down-tilt and $\beta < 0$ corresponds to an up-tilt with respect to the horizon). The von Mises distribution is given by

$$p(\theta) = \frac{1}{2\pi I_0(\kappa)} \exp\left[\kappa \cos(\theta - \beta)\right], \qquad (9)$$

where $I_0(\kappa)$ is the zero-order modified Bessel function, and κ can be regarded as an antenna directivity parameter. It is obvious that various antenna patterns have different influences on the joint (or separate) AOA and TD signal distributions at the receiver. To reflect this influence, let us examine the PDFs $p(\theta)$ from Equation (9) and $\mu_{fin}(\tau, \varphi)$ from Equation (8). These two distributions are independent, and, as was shown in [14], their combination gives a three-dimensional joint PDF in the AOA-TD, EOA-AOA, and EOA-TD planes:

$$\mu_{fin\_with\_elev}(\tau, \varphi, \theta) = \mu_{fin}(\tau, \varphi)\, p(\theta). \qquad (10)$$

We notice that Equation (10) is a general description of the directive antenna pattern, both in the vertical and horizontal planes. It fully represents the joint AOA, EOA, and TD distribution of the signal arriving at the receiver, affected by an array of obstructions surrounding the base-station and mobile-station terminal antennas.

3. Numerical Simulation versus Results of Measurements

Next, we compare some of the numerical simulations of the joint AOA, EOA, and TD distributions described by Equation (10) with the three-dimensional high-resolution measurements of the spatial radio channel, carried out in different scenarios in the city of Helsinki.

3.1 Microcell Radio Environment: Receiving Antenna Below Rooftops

One of the urban scenarios used in the experiment is shown in Figure 2. The parameters of this experiment were as follows:

- Minimum traffic on the streets
- The transmitting antenna was at street ground level (its height was about 2 m).
- The receiving antenna array was located at the level of the third floor of a neighboring building, but below the rooftop level (the height was about 10 m).
- The 3 dB field-of-view for the receiving antenna was 70° in both the azimuth and elevation planes.
- The transmitting antenna was omnidirectional in the azimuth and had an 87° beamwidth in the elevation domain.
- A wideband (100 MHz) channel sounder was used, with a carrier frequency of 2.154 GHz [9].

Let us now examine the resulting image for the joint AOA and TD distribution received by post-processing of the measured data, shown in Figure 3, and the resulting image received by using Equation (10), shown in Figure 4. Using the topographic map of the experimental site in Figure 2, we determined the parameters of the terrain to be $\gamma_0 = 4\ \text{km}^{-1}$, $h_1 \approx 10$ m, and $h_2 = 21$ m (i.e., $\bar{h} \approx 15$ m and $\chi = 0.5$). The wavelength and the range between terminals were $\lambda = 0.13$ m and $d = 0.3$ km, respectively. Figures 3, 7, and 9 show the probability distributions of the scattered waves arriving at the receiver. The concentration of rays in the AOA-TD plane was shown to vary from a maximum (0.5 to 0.9) to a minimum (0.1 to 0.4). From Figure 3, more than 80%-90% of the rays arrived at the receiver from two streets (due to the guiding effect of streets), i.e., by multiple reflections from buildings located along the streets.

Figures 3 and 4 show that despite the fact that the dominant number of rays (more than 80%) arrived due to the guiding effect of streets, there were still a number of arrivals (about 15%-20%) that were coming from different directions and symmetrical with respect to the pseudo-LOS direction. This result was clearly seen using Equation (10) for the case where both the transmitting and receiving antennas were below the rooftop level.

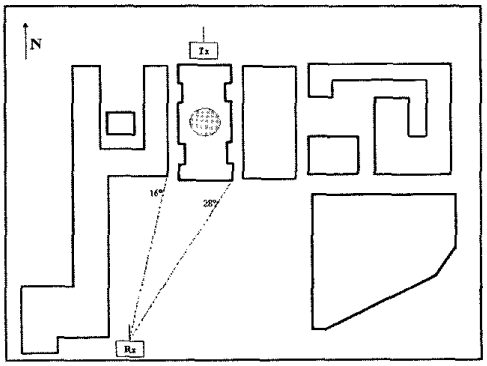

Figure 2. A micro-cell urban environment (the receiver is below the rooftop level).

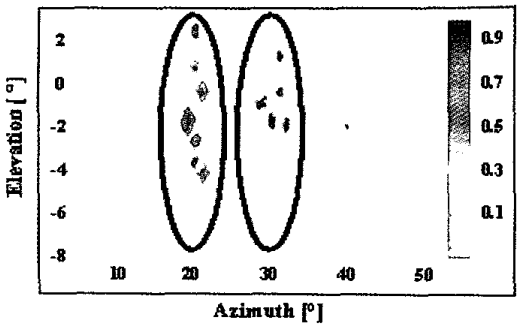

Figure 8. The measurements in the EOA-AOA plane: the antenna is below the rooftops.

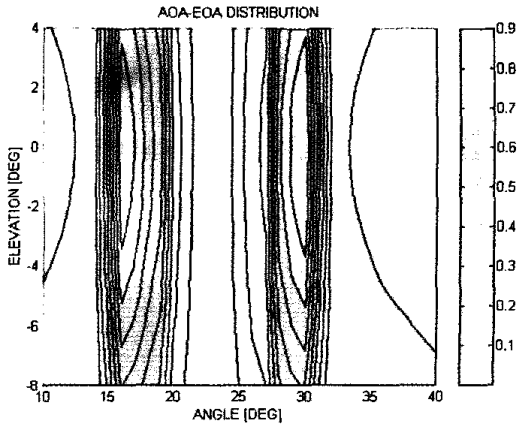

Figure 9. The simulation results for the joint PDF: the antenna is below the rooftops.

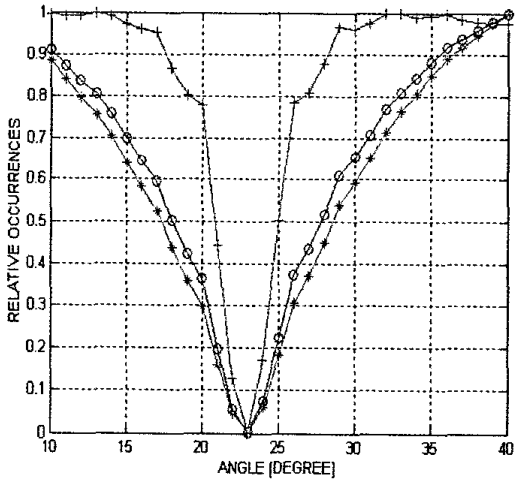

Figure 10. The AOA distribution as a function of the base-station mobile-station distance, without the guiding effect.

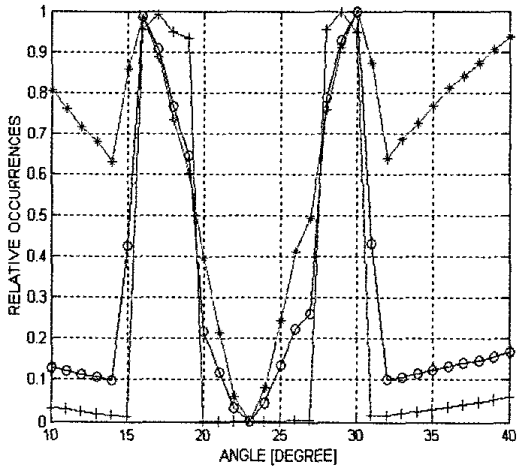

Figure 11. The AOA distribution depended on the base-station mobile-station distance: waveguide effect.

3.2 Microcell Radio Environment: Receiving Antenna at the Rooftop Level

Let us now introduce another set of measurements where the receiving antenna was at the rooftop level. For this experiment, shown in Figure 5, the following parameters were used:

- The transmitting antenna was at street ground level, with a height of 2 m.
- The receiving antenna, with height of 27 m, was located at the rooftop level near a building's corner.
- The 3 dB beamwidth of the transmitting antenna was 70° in the azimuth and elevation planes.
- The receiving antenna was omnidirectional in azimuth, and had an 87° beamwidth in the elevation plane. As in the previous case, there was no direct LOS between the transmitting and receiving antennas.
- The pseudo-LOS distance was about 420 m. One wide street was located at an azimuth angle of –30° degrees from the main lobe of the receiving antenna.

Using the topographic map of the experimental site in Figure 2, we determined the parameters of the terrain to be $\gamma_0 = 8\ \text{km}^{-1}$, $h_1 = 10$ m, and $h_2 = 29$ m (i.e., $\bar{h} \approx 19$ m and $\chi = 0.7$). The wavelength and the range between terminals were $\lambda = 0.13$ m and $d = 0.42$ km, respectively.

Figure 6 shows the resulting image of the post-processed measured data for the area shown in Figure 5, and Figure 7 shows the resulting image obtained using Equation (10). Once again, a good agreement between measured data and simulation results was observed. We must note, however, that our model cannot separately show two groups of arrivals as in Figure 6, which was characterized by a common azimuth range of –25° to –30° and different time delays. At the same time, our model takes into account all arrivals from the waveguide (street), assuming a straight-street-grid plan.

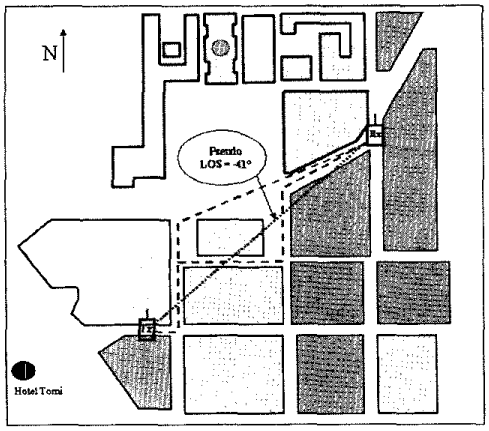

Figure 5. A micro-cell urban environment (the receiver is on the rooftop level).

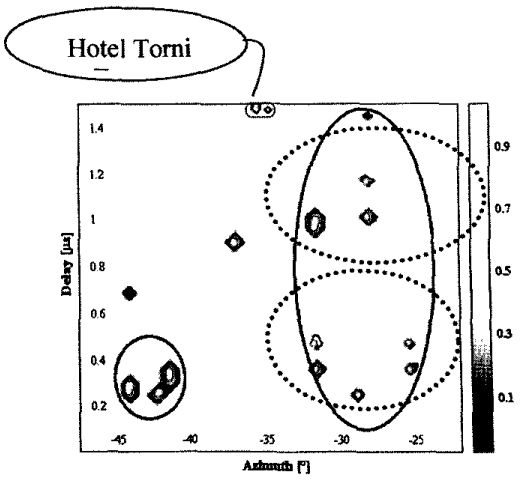

Figure 6. The measurement results: the antenna is on the rooftop level.

In the third case, shown in Figure 5, there were some differences in results between experimental data and Equation (10). These differences are illustrated in Figures 6 and 7. For such an urban scenario, a simple stochastic model, described by Equation (2), may be a better fit for the experimental data.

In this case, we could not match the arrivals from rays reflected from the high tower (Hotel Torni, shown in Figure 5). The reason for this is due to our basic assumption that in the azimuth plane we cannot see the building height distribution between h_1 and h_2, which are the minimum and maximum building heights in the area of investigation.

3.3 Antenna Directivity and Tilt Effects

Next, the effects of directivity and antenna tilt angle is presented, based on numerical simulations of the general three-dimensional Equation (10).

3.3.1 Joint AOA-EOA Distribution: Measurement and Simulation

Figure 8 depicts the results for the joint AOA-EOA distribution measured in the urban case described in Figure 2. Measurements showed that the rays were arriving within the elevation angular range of –4° to +2°, with most of the rays coming from the two street canyons caused by the guiding effect. Figure 9 shows the simulation results of the general three-dimensional case from Equation (10). A good agreement between measurement and simulation results was also observed in the AOA-EOA plane. Simulation results showed that most of the arrivals were concentrated within the elevation angular range of ±2° (see Figures 8 and 9). In fact, this result explains the over-rooftop propagation mechanism (in our example, the receiving antenna was at the

rooftop level). It means that the height of the buildings placed closest to the receiver define the elevation angles of arrival at the receiving antenna. This spreading of the number of arrivals, which is close to the zero elevation angle, was observed only from rays located along these two streets, where the guiding effects were observed in the azimuth domain (see Figures 8 and 9).

3.3.2 AOA Distance Dependence

Let us now analyze the behavior of the expressions in Equations (8)-(10), obtained by the stochastic approach, using the results from experiments in [1, 2, 7, 9]. It was shown in [1, 2] that the azimuth spread depends on the distance between the transmitting and receiving antennas in a specific manner. This dependence is also predicted by Equation (10). Furthermore, one can see that the angular spread is reduced when the distance (between transmitter and receiver) is increased, for certain situations. We analyzed two cases to confirm the empirical results obtained in [1, 2].

The first case, shown in Figure 10, related to the situation where there was no guiding effect, because the street-plan grid did not have a completely rectangular form. The second case, shown in Figure 11, related to the regular urban environment where there was a straight-line street grid. The urban case shown in Figure 2 was taken as a test case for our quantitative analysis. The azimuth of the pseudo-LOS direction between the transmitting and receiving antennas was about 23°. The different lines depict the different distances between the two antennas. A "*"curve was for a separation distance of 0.2 km, the "o" line was for a distance of 0.6 km, and the "+" line was for a distance of 2 km.

Figures 10 and 11 show that the angular spread decreased as the distance between the terminal antennas, base station, and mobile station increased. Figure 10 shows an interesting phenomenon: with an increase in the distance between the mobile-station and base-station antennas, the guiding effect became more dominant. The same results were observed in Helsinki for urban scenarios that included a straight-grid street plan [9].

4. Summary

In this work, we addressed the problem of modeling the joint AOA-TD, EOA-TD, and EOA-AOA signal distributions in different areas in the city of Helsinki. In this model, we considered arrays of buildings randomly distributed and arrays of streets with a straight-line grid plan. A comparison of theoretical and experimental results showed very good agreement for the cases where the receiving antenna was below the rooftop level or at the same level. It was found both theoretically and experimentally that for the dense Helsinki areas, up to 85%-95% of the total received rays propagated along the streets. The dependence of the AOA on the receiver-transmitter distance was also confirmed by the proposed combined stochastic and waveguide models.

5. References

1. K. I. Pedersen, P. Mogensen, and B. H. Fleury, "A Stochastic Model of the Temporal and Azimuthal Dispersion Seen at the Base Station in Outdoor Propagation Environments," *IEEE Transactions on Antennas and Propagation*, **AP-49**, 2000, pp. 437-447.

2. K. I. Pedersen, P. Mogensen, and B. H. Fleury, "Experimental Analysis of the Joint Statistical Properties of Azimuth Spread, Delay Spread, and Shadow Fading," *IEEE Journal on Selected Areas of Communications*, **20**, 3, 2002, pp. 523-531.

3. Q. Spencer, "Modeling the Statistical Time and Angle-of-Arrival Characteristics of an Indoor Multipath Channel," *IEEE Journal on Selected Areas of Communications*, **18**, 2, 2000, pp. 347-360.

4. J. B. Andersen and K. I. Pedersen, "Angle-of-Arrival Statistics for Low Resolution Antennas," *IEEE Transactions on Antennas and Propagation*, **AP-50**, 3, 2002, pp.391-395.

5. C. Cheon, G. Liang, and H. L. Bertoni, "Simulating Radio Channel Statistics for Different Building Environments," *IEEE Journal on Selected Areas of Communications*, **19**, 11, 2001, pp. 2191-2200.

6. C. Kloch, G. Liang, J. B. Andersen, G. F. Pedersen, and H. L. Bertoni, "Comparison of Measured and Predicted Time Dispersion and Direction of Arrival for Multipath in a Small Cell Environment," *IEEE Transactions on Antennas and Propagation*, **AP-49**, 9, 2001, pp. 1254-1263.

7. A. M. Saleh and R. A. Valenzula, "A Statistical Model for Indoor Multipath Propagation," *IEEE Journal on Selected Areas of Communications*, **5**, 1987, pp. 128-137.

8. N. Blaunstein, "Average Field Attenuation in the Nonregular Impedance Street Waveguide," *IEEE Transactions on Antennas and Propagation*, **AP-46**, 12, 1998, pp. 1782-1789.

9. N. Blaunstein, "Distribution of Angle-of-Arrival and Delay from Array of Buildings Placed on Rough Terrain for Various Elevations of Base Station Antenna," *J. Communication and Networks*, **2**, 4, 2000, pp. 305-316.

10. J. Fuhl, J.-P. Rossi, and E. Bonek, "High-Resolution 3-D Direction-of-Arrival Determination for Urban Mobile Radio," *IEEE Transactions on Antennas and Propagation*, **AP-45**, 4, 1997, pp. 672-683.

11. J. Laurila , K. Kalliola, M. Toeltsch, K. Hugl, P. Vainikainen, and E. Bonek, "Wide-Band 3-D Characterization of Mobile Radio Channels in Urban Environment," *IEEE Transactions on Antennas and Propagation*, **AP-50**, 2, 2002, pp. 233-243.

12. M. Toeltsch, J. Laurila, K. Kalliola, A. F. Molisch, P. Vainikainen, and E. Bonek," Statistical Characterization of Urban Spatial Radio Channels," *IEEE Journal on Selected Areas of Communications*, **20**, 3, 2002, pp. 539-549.

13. K. Kalliola, H. Laitinen, P. Vainikainen, M. Toeltsch, J. Laurila, and E. Bonek, "3-D Double-Directional Radio Channel Characterization for Urban Macro Cellular Applications," *IEEE Transactions on Antennas and Propagation*, **AP-51**, 2003, pp.3122-3133.

14. N. Blaunstein, and E. Tsalolihin, "Signal Distribution in the Azimuth, Elevation, and Time Delay Domains in Urban Radio Communication Links," *IEEE Antennas and Propagation Magazine*, **46**, 5, 2004, pp. 171-178.